Market Scheduling and Pricing for Comprehensive Frequency Regulation Services

Yihang Jiang and Shuqiang Zhao

Abstract—**The increasing integration of renewable energy sources poses great challenges to the power system frequency security. However, the existing electricity market mechanism lacks integration and incentives for emerging frequency regulation (FR) resources such as wind power generators (WPGs), which may reduce their motivation to provide frequency support and further deteriorate the frequency dynamics. In this paper, a market scheduling and pricing method for comprehensive frequency regulation services (FRSs) is proposed. First, a modeling approach for flexible FR capabilities of WPGs is proposed based on the mechanism of inertia control and power reserve control. Subsequently, considering the differences in inverter control strategies, a novel system frequency response model with grid-following and grid-forming inverters is established. Combined with the automatic generation control, the frequency security constraints of the whole FR process are derived, and integrated into the market scheduling model to co-optimize the energy and FRSs. Finally, by distinguishing the contributions of various types of resources in different FR stages, a differentiated pricing scheme is proposed to incentivize producers with various regulation qualities to provide FRSs. The effectiveness of the proposed method is verified on the modified IEEE 6-bus system and the IEEE RTS-79 system.**

Index Terms—**Market scheduling, wind power generator (WPG), frequency support, frequency regulation, frequency response, grid-forming inverter, pricing, frequency security.**

I. Introduction

As a promising technology for reducing carbon emissions, a large number of renewable energy sources (RESs), represented by wind power generators (WPGs), have been integrated into the power system, posing great challenges to system security and stability [1]. One of the main problems recognized is the deterioration of the system frequency dynamics due to the reduction of inertia and frequency regulation (FR) reserve [2], since the non-synchronous grid connection of WPGs [3]. Historically, the electricity market design has focused on the FR capabilities of conventional generators, which inherently provided both inertia and FR reserves [4]. However, with the development of advanced control strategies, WPGs can now actively participate in FR through appropriate control of the inverters [5], [6]. This shift in technological capabilities calls for a gradual adaptation of market mechanisms to account for the FR provision of WPGs. As such, the procurement of frequency regulation services (FRSs) from WPGs to ensure system frequency stability in future inverter-based power systems remains an unresolved challenge.

Some studies have been conducted to develop market clearing procedures for the clearing and pricing of various FRSs, usually unit commitment (UC) or economic dispatch (ED) models that include frequency security constraints. Reference [7] proposed a scheduling method for simultaneous clearing of energy, primary, secondary, and tertiary reserves. References [8] and [9] presented a market design for scheduling and pricing synchronous inertia as well as primary frequency regulation (PFR) service. As an extension of the above research, [10] explored the frequency evolution in the process of PFR and secondary frequency regulation (SFR), adopted the methodology proposed in [11] to model the system frequency dynamics in a more detailed way, and proposed a locational reserve pricing method to differentiate the procurement prices of different nodes. In [12], a dynamic-aware ED was proposed to investigate the impact of system frequency dynamics on the real-time locational marginal price (LMP). The above studies provide references for the design of the FR market, but none of them considers the share of frequency support provided by WPGs.

This has been noted in recent research, where [13] provided a techno-economic analysis of the profitability of WPGs as potential participants in the SFR market. Reference [14] introduced the synthetic inertia and droop factors of WPGs and designed a market mechanism that accounts for inertia and PFR with consideration of the energy market. In [15], a chance-constrained stochastic UC model was developed to investigate the impact of WPG uncertainty on inertia prices, while only the minimum inertia requirement constraint was included. Reference [16] proposed a frequency-constrained unit commitment (FCUC) model for the simultaneous clearing of FRSs with diverse response speeds and developed a corresponding marginal pricing scheme based on mixed-integer second-order cone programming. Recent research also introduced novel automatic generation control (AGC) strategies to account for the FR provision of WPGs. An adaptive

Manuscript received: July 20, 2024; revised: November 21, 2024; accepted: December 17, 2024. Date of CrossCheck: December 17, 2024. Date of online publication: January 3, 2025.

This work was supported by the National Key Research and Development Program of China (No. 2023YFB2406800).

Y. Jiang (corresponding author) and S. Zhao are with the State Key Laboratory of Alternate Electrical Power System with Renewable Energy Sources, North China Electric Power University, Beijing 102206, China (e-mail: yh_jiang2000@163.com; zsqdl@163.com).

DOI: 10.35833/MPCE.2024.000771

distributed auction-based algorithm for optimal mileage-based AGC dispatch with high participation of RESs was proposed in [17], and a distributed event-triggered fixed-time sliding-mode control-based AGC for power systems with heterogeneous FR units was introduced in [18].

The above studies provide valuable insights. Indeed, owing to the flexible controllability of power electronics, WPGs offer faster frequency response speeds and flexible FRSs [19] and can participate in the FR market as enhanced frequency regulation (EFR) services [20]. However, in most previous studies, the frequency support capability of WPGs is simply modeled as a fixed inertia constant or PFR factor, which may affect the market competitiveness of WPGs. Some factors should also be properly considered to enhance the accuracy of market scheduling results, e.g., WPGs must be deloaded to reserve power for PFR and SFR [21], necessitating a trade-off between the energy market and the FR market. In addition, the detailed modeling of the whole process of frequency evolution and the coupling relationship among inertia response (IR), PFR, and SFR has not been fully investigated.

Moreover, WPGs can be categorized into two types according to the differences in the control of grid-connected inverters, i.e., grid-following (GFL) inverter and grid-forming (GFM) inverter [22]. The GFL inverter tracks the system frequency through a phase-locked loop to achieve synchronization. Due to the inherent measurement delay, it does not contribute to the initial rate of change of frequency (RoCoF) although it can improve the frequency dynamics [23]. The GFM inverter is a better choice because it has manners similar to synchronous generators as a voltage source [24]. However, almost all existing WPGs are equipped with GFL inverters, and producers lack a clear motivation to deploy GFM inverters because there is no effective market mechanism to provide economic incentives, and almost none of the previous studies has distinguished the differences between the two. The most relevant work is in [25], where it is argued that the GFL inverter provides only EFR service. However, the inertia provided by the GFL inverters is still valuable, as it can act to improve the frequency nadir, which is determined by a combination of the system inertia as well as the PFR.

Given this background, a market scheduling and pricing method for comprehensive FRSs is proposed. The main challenge addressed in this paper is how to model and schedule FR resources with varying regulation quality and response characteristics, and design a rational pricing mechanism reflecting their respective contributions, thereby incentivizing their participation in the market. The main contributions are three-fold:

1) Based on the mechanism of inertia control and power reserve control (PRC), a modeling approach for flexible FR capabilities of WPGs is proposed. Subsequently, the system frequency response model (SFRM) that includes the thermal generators (TGRs) and the WPGs equipped with GFL inverters and GFM inverters is established.

2) Combining the SFRM and AGC mechanism, the key frequency security constraints from IR to SFR are derived and incorporated into the market scheduling model to co-optimize the energy and FRSs. A modified piece-wise linearization (PWL) algorithm is adopted to deal with the non-convex constraints.

3) The contributions of GFM and GFL inertia and the differences in PFR and EFR response speed are distinguished. Combined with the contribution of each type of resource in the whole FR process, a differentiated pricing scheme is proposed to incentivize FR resources with different regulation qualities to participate in the market.

The rest of this paper is organized as follows. Section II introduces the modeling of system frequency dynamics and the derivation of frequency security constraints. The market scheduling model for comprehensive FRSs and the modified PWL algorithm are discussed in Section III. The differentiated pricing scheme is presented in Section IV. Section V discusses the results of several case studies, while Section VI concludes the paper.

II. Modeling of System Frequency Dynamics and Derivation of Frequency Security Constraints

A. Modeling of Flexible FR Capabilities of WPGs

The simplified mechanical and aerodynamic model of WPGs can be expressed as [26]:

$$\begin{cases} J^{\mathrm{W}}\omega_{\mathrm{r}}\dfrac{\mathrm{d}\omega_{\mathrm{r}}}{\mathrm{d}t}=P_{\mathrm{m}}-P_{\mathrm{e}} \\ P_{\mathrm{m}}=\dfrac{1}{2}\rho\pi R^{2}v_{\mathrm{w}}^{3}C_{\mathrm{p}}(\omega_{\mathrm{r}},\beta^{\mathrm{w}}) \end{cases} \tag{1}$$

where J^{W} is the inertia of the WPG driven system; P_{m} and P_{e} are the mechanical and electrical power of WPG, respectively; ρ, R, and v_{w} are the air density, WPG blade radius, and wind speed, respectively; and $C_{\mathrm{p}}(\omega_{\mathrm{r}},\beta^{\mathrm{w}})$ is the power coefficient of WPGs, which is dependent on the rotor speed ω_{r} and the pitch angle β^{w}. When a power loss disturbance occurs, the WPG with the additional inertia control loop rapidly releases the rotor kinetic energy and injects energy into the power system, and this dynamic process can be represented by [27]:

$$J^{\mathrm{W}}\omega_{\mathrm{r}}\frac{\mathrm{d}\omega_{\mathrm{r}}}{\mathrm{d}t}=P_{\mathrm{m}}-P_{\mathrm{e}}=2H^{\mathrm{WT}}\frac{\mathrm{d}\Delta f(t)}{\mathrm{d}t} \tag{2}$$

where H^{WT} is the synthetic inertia provided by WPG; and $\Delta f(t)$ is the system frequency deviation. By integrating the left and right sides of (2), the inertia can be calculated and expressed as:

$$H^{\mathrm{WT}}=\frac{J^{\mathrm{W}}(\omega_{\mathrm{r0}}^{2}-\omega_{\mathrm{r}}^{2})}{4\Delta f(t)} \tag{3}$$

where ω_{r0} is the pre-disturbance rotor speed. In the practical FR process, the WPG is constrained by security operation limits, resulting in the actual release of inertia unable to reach the theoretical maximum. The main constraints include rotor speed limit and inverter capacity limit, which can be expressed as:

$$\omega_{\mathrm{rmin}}\leq\omega_{\mathrm{r}}\leq\omega_{\mathrm{rmax}} \tag{4}$$

$$P_{\mathrm{e}}\leq P_{\mathrm{max}}^{\mathrm{I}} \tag{5}$$

where ω_{rmax} and ω_{rmin} are the maximum and minimum rotor speed limits, respectively; and $P_{\max}^{\text{I}}$ is the maximum inverter capacity. When designing the frequency control parameters of the WPG, the system frequency security limits are usually considered to represent the inertia requirements of the system [28]. Accordingly, the maximum available inertia of the WPG can be derived as:

$$H^{\text{WT}} = \min\left\{\frac{J^{\text{W}}(\omega_{\text{r0}}^2-\omega_{\text{rmin}}^2)}{4\left|\Delta f_{\max}\right|}, \frac{P_{\max}^{\text{I}}-P_0^{\text{W}}}{2\left|RoCoF_{\max}\right|}\right\} \tag{6}$$

where P_0^{W} is the pre-disturbance power output of the WPG; and $RoCoF_{\max}$ and $\Delta f_{\max}$ are the maximum allowable RoCoF and frequency deviation of the system, respectively. Figure SA1 in Supplementary Material A depicts the calculation results under full wind speed conditions. It can be observed that H^{WT} rises rapidly after the cut-in wind speed, then decreases and remains constant due to the inverter capacity limit. Subsequently, the equivalent inertia time constant $H_{\text{s},w}^{\text{W}}$ of a wind farm (WF) can be aggregated based on the wind speed distribution as:

$$H_{\text{s},w}^{\text{W}} = \frac{\left(\int_0^{\infty} N_m H_m^{\text{WT}} \cdot wd_m(v_{\text{w}})\text{d}v_{\text{w}}\right) f_{\text{n}}}{S_w^{\text{W}}} \tag{7}$$

where N_m is the number of WPGs in the WF; H_m^{WT} is the inertia of the m^{th} WPG; wd_m is the wind speed distribution of the m^{th} WPG; f_{n} is the nominal frequency of the system; and S_w^{W} is the installation capacity of WF. In the subsequent PFR and SFR process, the WPGs participate in the FR by releasing the active power generated by the PRC. Define the deloading rate d_w^{W} as the key decision variable for PRC, the relationship between the maximum power point track (MPPT) power $P_w^{\text{W,MPPT}}$ and the deloaded power $P_w^{\text{W,del}}$ after adopting PRC can be expressed as:

$$P_w^{\text{W,del}} = (1-d_w^{\text{W}})P_w^{\text{W,MPPT}} \tag{8}$$

When the system frequency exceeds the deadband, the active power output for FR is increased by WPGs according to a pre-defined droop factor R_w^{W}, which is set in conjunction with the deloading rate, as given in (9).

$$1/R_w^{\text{W}} = d_w^{\text{W}} P_w^{\text{W,MPPT}}/\Delta f_{\max} \tag{9}$$

In addition, it should be noted that the decrease in the captured mechanical power efficiency due to the reduction of rotor speed after the IR is modeled as a rotor speed reduction factor δ in our previous work [29]. This also indicates the lost opportunity cost of WPGs in PFR or SFR in order to provide inertia. The expression for the modified droop factor is given as:

$$1/R_w^{\text{W}} = (1-\delta)d_w^{\text{W}} P_w^{\text{W,MPPT}}/\Delta f_{\max} \tag{10}$$

B. Frequency Dynamics and Security Constraints of Whole FR Process

1) IR and PFR Stage

Consider a typical power system with TGRs and WPGs equipped with GFL inverters and GFM inverters, of which the SFRM is shown in Fig. 1.

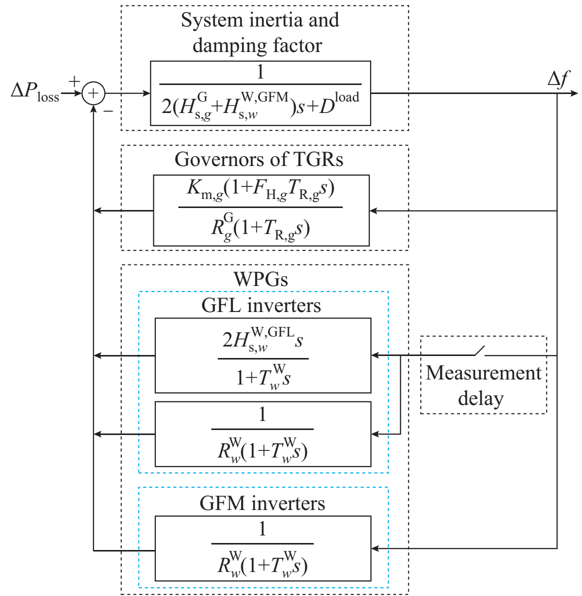

Fig. 1. SFRM of a typical power system with TGRs and WPGs equipped with GFM inverters and GFL inverters.

In the IR and PFR stage, the main frequency security metrics include the RoCoF, the frequency nadir Δf_{nadir}, and the quasi-steady-state (QSS) frequency deviation Δf_{QSS}. For a given frequency disturbance ΔP_{loss}, the initial RoCoF is only related to the inertia provided by TGRs and GFM inverters, and the inertia provided by GFL inverters has no contribution due to the inherent measurement delay. Accordingly, the initial RoCoF constraint is firstly obtained as:

$$RoCoF = \frac{\Delta P_{\text{loss}}}{2\left(\sum_{g\in\phi_{\text{g}}} H_{\text{s},g}^{\text{G}} + \sum_{w\in\phi_{\text{GFM}}} H_{\text{s},w}^{\text{W,GFM}}\right)} \le RoCoF_{\max} \tag{11}$$

where $H_{\text{s},g}^{\text{G}}$ and $H_{\text{s},w}^{\text{W,GFM}}$ are the inertia provided by TGRs and GFM inverters, respectively; and ϕ_{g} and ϕ_{GFM} are the sets of TGRs and GFM inverters, respectively. In the subsequent derivation, the measurement delay (typically 100 ms) is neglected because its effect on the frequency nadir as well as on the QSS frequency deviation is small, given that the governor time constant of TGRs is usually several orders of magnitude larger. The specific effect of neglecting measurement delay is analyzed in Supplementary Material B. The inverter time constant of WPG T_w^{W} is neglected for the same reason as the measurement delay. Based on this assumption and assuming a step-wise disturbance in ΔP_{loss}, the transfer function $G(s)$ of SFRM is obtained as:

$$G(s) = \frac{\Delta f}{\Delta P_{\text{loss}}} = \left[2s\left(\sum_{g\in\phi_{\text{g}}} H_{\text{s},g}^{\text{G}} + \sum_{w\in\phi_{\text{GFM}}} H_{\text{s},w}^{\text{W,GFM}} + \sum_{w\in\phi_{\text{GFL}}} H_{\text{s},w}^{\text{W,GFL}}\right) + \left(D^{\text{load}} + \sum_{w\in\phi_{\text{GFL}}\cup\phi_{\text{GFM}}} \frac{1}{R_w^{\text{W}}}\right) + \sum_{g\in\phi_{\text{g}}} \frac{K_{\text{m},g}(1+sF_{\text{H},g}T_{\text{R},g})}{R_g^{\text{G}}(1+sT_{\text{R},g})}\right]^{-1} \tag{12}$$

where D^{load} is the load damping factor; $K_{\text{m},g}$, $F_{\text{H},g}$, $T_{\text{R},g}$, and R_g^{G} are the mechanical power gain factor, fraction of power generated by the high-pressure turbine, reheater time constant, and governor regulation constant, respectively; $H_{s,w}^{W,GFL}$ is the inertia provided by GFL inverters; and ϕ_{GFL} is the set of GFL inverters. Then the time-domain expression for the system frequency evolution is obtained by applying the inverse Laplace transform to (12) as:

$$\Delta f(t)=\frac{\Delta P_{loss}}{D^{sys}+R^{G}}\left(1+\alpha e^{-\zeta\omega_n t}\sin(\omega_r t+\varphi)\right) \tag{13}$$

$$\begin{cases} \omega_n^2=(D^{sys}+R^{G})/(2H_s^{sys}T_R) \\ \omega_r=\omega_n\sqrt{1-\zeta^2} \\ \zeta=\dfrac{D^{sys}T_R+2H_s^{sys}+F_H T_R}{2(D^{sys}+R^{G})}\omega_n \\ \alpha=\sqrt{(1-2T_R\zeta\omega_n+T_R^2\omega_R^2)/(1-\zeta^2)} \\ \varphi=\arctan\left(\dfrac{\omega_r T_R}{1-\zeta\omega_n T_R}\right)-\arctan\left(-\dfrac{1}{\zeta}\sqrt{1-\zeta^2}\right) \end{cases} \tag{14}$$

$$\begin{cases} H_s^{sys}=\dfrac{\sum\limits_{g\in\phi_g}u_g^G H_{s,g}^G S_g^G+\sum\limits_{w\in\phi_{GFM}}H_{s,w}^{W,GFM}S_w^W+\sum\limits_{w\in\phi_{GFL}}H_{s,w}^{W,GFL}S_w^W}{S_{total}} \\ F_H=\dfrac{\sum\limits_{g\in\phi_g}u_g^G K_{m,g}F_{H,g}S_g^G/R_g^G}{S_{total}} \\ R^G=\dfrac{\sum\limits_{g\in\phi_g}u_g^G K_{m,g}S_g^G/R_g^G}{S_{total}} \\ R^W=\dfrac{\sum\limits_{w\in\phi_{GFM}\cup\phi_{GFL}}S_w^W/R_w^W}{S_{total}} \\ T_R=\dfrac{\sum\limits_{g\in\phi_g}u_g^G K_{m,g}T_{R,g}S_g^G/R_g^G}{S_{total}} \\ D^{sys}=\dfrac{D^{load}P^L+R^W S_{total}}{S_{total}} \end{cases} \tag{15}$$

where D^{sys} is the system damping term with the provision from the system load and WPGs; R^G is the aggregated governor regulation constant of TGRs; the detailed meanings of ζ, ω_n, ω_r, α, and φ can be found in [30]; F_H and T_R are the aggregated fractions of power generated by the high-pressure turbine and the aggregated reheater time constant, respectively; H_s^{sys} is the aggregated system inertia with the provision from TGRs, GFL inverters, and GFM inverters; R^W is the aggregated droop factor of WPGs; u_g^G is the binary decision variable indicating the on-off status of TGRs; S_g^G is the installed capacity of a single TGR; S_{total} is the total generator installed capacity of the system; and P^L is the system load demand. At the moment of frequency nadir, the RoCoF reaches zero, i.e., $\partial\Delta f(t)/\partial t=0$. Based on this relationship, the system frequency nadir deviation constraint is obtained as:

$$\Delta f_{nadir}=\frac{\Delta P_{loss}}{D^{sys}+R^{G}}\left(1+\sqrt{1-\zeta^2}\,\alpha e^{-\zeta\omega_n t_{nadir}}\right)\le\Delta f_{max} \tag{16}$$

where Δf_{nadir} is the system frequency nadir deviation; and $t_{nadir}=\arctan(\omega_r T_R/(\zeta\omega_r T_R-1))/\omega_r$ is the time at which the frequency reaches the nadir. Finally, the QSS frequency deviation constraint is obtained by applying the final-value theorem to (13) as:

$$\Delta f_{QSS}=\frac{\Delta P_{loss}}{D^{sys}+R^{G}}\le\Delta f_{QSS}^{max} \tag{17}$$

where Δf_{QSS} and Δf_{QSS}^{max} are the QSS frequency deviation and its maximum allowable value, respectively.

Remark It can be noticed that the droop factors of WPGs in (15) are endogenously aggregated to the system damping term, which is different from [31] and other studies that uniformly aggregate them with droop factors of TGRs. The approach proposed in [31] may fail to distinguish the fast regulation characteristics of WPGs as EFR due to the influence of the governor time constant of TGRs.

2) SFR Stage

After the PFR stage, the AGC acts to restore the frequency to its nominal value. The AGC typically adjusts the output reference of the selected generators to offset the power imbalance and restores the output of the remaining non-AGC generators to their original values. According to the North American Electric Reliability Council [32], the area control error (ACE) must reach zero within 10 min or it will be ruled as a violation, so the SFR service is usually a 10-min product. The ACE can be calculated as:

$$ACE=\Delta f_{QSS}\beta_1+\Delta P_{tie}=-\Delta P_{loss} \tag{18}$$

$$\Delta P_{tie}=-\Delta P_{loss}\beta_2/(\beta_1+\beta_2) \tag{19}$$

where β_1 and β_2 are the frequency response characteristics of the internal and external areas, respectively; and ΔP_{tie} is the steady-state tie-line transmission power. At the beginning of the SFR, generators in the system have already increased a certain amount of power output for PFR, which is forced to be maintained during the SFR process [10], as shown in Fig. 2.

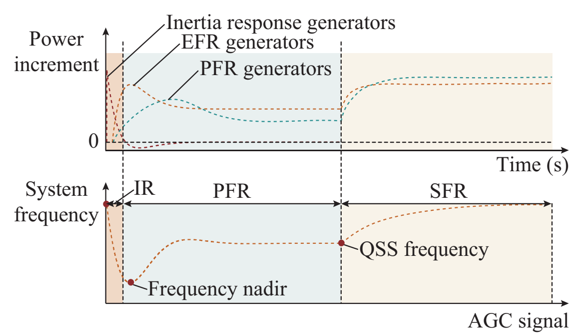

Fig. 2. Frequency dynamics of whole FR process after a power loss disturbance.

For each TGR, this power increment $PFR_g^{G,QSS}$ can be calculated as:

$$PFR_g^{G,QSS}=u_g^G K_{m,g}\Delta f_{QSS}/R_g^G \tag{20}$$

For WPG, the power increment $PFR_w^{W,QSS}$ is obtained as:

$$PFR_w^{W,QSS}=\Delta f_{QSS}/R_w^W \tag{21}$$

Accordingly, the SFR capacity SFR^{sys} to be deployed can be calculated as:

$$SFR^{\mathrm{sys}}=\Delta P_{\mathrm{loss}}-\sum_{g\in\phi_{\mathrm{g}}}PFR_{g}^{\mathrm{G,QSS}}-\sum_{w\in\phi_{\mathrm{w}}}PFR_{w}^{\mathrm{W,QSS}}=\Delta P_{\mathrm{loss}}-\Delta f_{\mathrm{QSS}}(R^{\mathrm{G}}+R^{\mathrm{W}}) \tag{22}$$

The constraints for the SFR process are derived as:

$$\sum_{g\in\phi_{\mathrm{g}}}SFR_{g}^{\mathrm{G}}+\sum_{w\in\phi_{\mathrm{w}}}SFR_{w}^{\mathrm{W}}\geq\Delta P_{\mathrm{loss}}-\Delta f_{\mathrm{QSS}}^{\max}(R^{\mathrm{G}}+R^{\mathrm{W}}) \tag{23}$$

$$SFR_{g}^{\mathrm{G}}\leq 10\cdot rr_{g} \tag{24}$$

$$P_{g}^{\mathrm{G}}+PFR_{g}^{\mathrm{G,QSS}}+SFR_{g}^{\mathrm{G}}\leq u_{g}^{\mathrm{G}}P_{g}^{\max} \tag{25}$$

$$P_{w}^{\mathrm{W}}+PFR_{w}^{\mathrm{W,QSS}}+SFR_{w}^{\mathrm{W}}\leq P_{w}^{\mathrm{W,MPPT}} \tag{26}$$

where SFR_{g}^{G} and SFR_{w}^{W} are the SFR reserves provided by TGRs and WPGs, respectively; P_{g}^{G} and P_{w}^{W} are the actual power outputs of TGRs and WPGs, respectively; $P_{g}^{\max}$ is the maximum power output of TGRs; and rr_{g} is the maximum SFR ramp rate of TGRs.

Formula (23) ensures that the SFR deployment capacity is sufficient. Formula (24) ensures that the SFR capacity provided by TGRs can be deployed within 10 min. Formulas (25) and (26) ensure that the TGRs and WPGs have sufficient power increment headroom. Also note that in some areas, the actual AGC regulation time may be less than 10 min, sometimes within 5 min [33]. While this does not affect the validity of our model, as it can be adapted to different requirements by modifying the specific parameters in (24).

III. Market Scheduling Model for Comprehensive FRSs and Modified PWL Algorithm

A. FCUC Model

The procedure used for clearing in this paper is a UC model that includes frequency security constraints to co-optimize energy and FRSs, as shown in (27)-(46). The objective function (27) contains only the start-up, shut-down, and operation costs of TGRs, excluding the bidding costs incurred by FRSs, as is also done in [10]. This setup is chosen because the primary focus of this paper is on the scheduling and pricing of energy and FRSs, and on ensuring that the results can accurately distinguish the contributions of generators. The bidding behaviors of generators are beyond the scope of this paper. Therefore, the prices for each type of ancillary service calculated in Section IV reflect only the lost opportunity costs of generators.

$$\min\sum_{t\in T}\sum_{g\in\phi_{\mathrm{g}}}(C_{g}(P_{g,t}^{\mathrm{G}})+SU_{g,t}+SD_{g,t}) \tag{27}$$

s.t.

$$u_{g,t}^{\mathrm{G}}P_{g}^{\min}\leq P_{g,t}^{\mathrm{G}}\leq u_{g,t}^{\mathrm{G}}P_{g}^{\max}\quad\forall t,\forall g \tag{28}$$

$$-RR_{g}\leq P_{g,t}^{\mathrm{G}}-P_{g,t-1}^{\mathrm{G}}\leq RR_{g}\quad\forall t,\forall g \tag{29}$$

$$\sum_{t=1}^{t+TS_{g}-1}(1-u_{g,t}^{\mathrm{G}})\geq TS_{g}\cdot(u_{g,t-1}^{\mathrm{G}}-u_{g,t}^{\mathrm{G}})\quad\forall t,\forall g \tag{30}$$

$$\sum_{t=1}^{t+TO_{g}-1}u_{g,t}^{\mathrm{G}}\geq TO_{g}\cdot(u_{g,t}^{\mathrm{G}}-u_{g,t-1}^{\mathrm{G}})\quad\forall t,\forall g \tag{31}$$

$$SU_{g,t}\geq su_{g}\cdot(u_{g,t}^{\mathrm{G}}-u_{g,t-1}^{\mathrm{G}})\quad\forall t,\forall g \tag{32}$$

$$SD_{g,t}\geq sd_{g}\cdot(u_{g,t-1}^{\mathrm{G}}-u_{g,t}^{\mathrm{G}})\quad\forall t,\forall g \tag{33}$$

$$\begin{cases}SU_{g,t}\geq 0\\ SD_{g,t}\geq 0\end{cases}\quad\forall t,\forall g \tag{34}$$

$$\sum_{g\in\phi_{\mathrm{g}}}P_{g,t}^{\mathrm{G}}+\sum_{w\in\phi_{\mathrm{w}}}P_{w,t}^{\mathrm{W}}=\sum_{n\in\phi_{\mathrm{n}}}P_{n,t}^{\mathrm{L}}\quad\forall t,\forall l \tag{35}$$

$$\sum_{n\in\phi_{\mathrm{n}}}PTDF_{n,l}\cdot(P_{g,n,t}^{\mathrm{G}}+P_{w,n,t}^{\mathrm{W}}-P_{n,t}^{\mathrm{L}})\leq F_{l}^{\max}\quad\forall t,\forall l \tag{36}$$

$$PFR_{g,t}^{\mathrm{G,nadir}}\geq u_{g,t}^{\mathrm{G}}K_{\mathrm{m},g}P_{g}^{\max}\sigma_{g}\Delta f_{\max}/R_{g}^{\mathrm{G}}\quad\forall t,\forall g \tag{37}$$

$$SFR_{g,t}^{\mathrm{G}}\leq 10\cdot rr_{g,t}\quad\forall t,\forall g \tag{38}$$

$$P_{g,t}^{\mathrm{G}}+PFR_{g,t}^{\mathrm{G,nadir}}\leq u_{g,t}^{\mathrm{G}}P_{g}^{\max}\quad\forall t,\forall g \tag{39}$$

$$P_{g,t}^{\mathrm{G}}+PFR_{g,t}^{\mathrm{G,QSS}}+SFR_{g,t}^{\mathrm{G}}\leq u_{g,t}^{\mathrm{G}}P_{g}^{\max}\quad\forall t,\forall g \tag{40}$$

$$P_{w,t}^{\mathrm{W}}=(1-d_{w,t}^{\mathrm{W}})P_{w,t}^{\mathrm{W,MPPT}}\quad\forall t,\forall w \tag{41}$$

$$0\leq P_{w,t}^{\mathrm{W}}+PFR_{w,t}^{\mathrm{W,QSS}}+SFR_{w,t}^{\mathrm{W}}\leq P_{w,t}^{\mathrm{W,MPPT}}\quad\forall t,\forall w \tag{42}$$

$$\frac{\Delta P_{\mathrm{loss},t}}{2\left(\sum_{g\in\phi_{\mathrm{g}}}H_{\mathrm{s},g}^{\mathrm{G}}+\sum_{w\in\phi_{\mathrm{GFM}}}H_{\mathrm{s},w}^{\mathrm{W,GFM}}\right)}\leq RoCoF_{\max}\quad\forall t \tag{43}$$

$$f_{\mathrm{n}}-\frac{\Delta P_{\mathrm{loss},t}}{D_{t}^{\mathrm{sys}}+R_{t}^{\mathrm{G}}}\left(1+\sqrt{1-\zeta^{2}}\,\alpha\mathrm{e}^{-\zeta\omega_{\mathrm{n}}t_{\mathrm{nadir}}}\right)\leq\Delta f_{\max}\quad\forall t \tag{44}$$

$$f_{\mathrm{n}}-\frac{\Delta P_{\mathrm{loss},t}}{D_{t}^{\mathrm{sys}}+R_{t}^{\mathrm{G}}}\leq\Delta f_{\mathrm{QSS}}^{\max}\quad\forall t \tag{45}$$

$$\sum_{g\in\phi_{\mathrm{g}}}SFR_{g,t}^{\mathrm{G}}+\sum_{w\in\phi_{\mathrm{w}}}SFR_{w,t}^{\mathrm{W}}\geq\Delta P_{\mathrm{loss},t}-\Delta f_{\mathrm{QSS}}^{\max}(R_{t}^{\mathrm{G}}+R_{t}^{\mathrm{W}})\quad\forall t \tag{46}$$

where T is the set of scheduling time periods; $C_{g}(P_{g,t}^{\mathrm{G}})$ is the cost function of TGRs; $SU_{g,t}$ and $SD_{g,t}$ are the start-up and shut-down costs of TGRs at time t, respectively; $P_{g,t}^{\mathrm{G}}$ and $P_{w,t}^{\mathrm{W}}$ are the actual power outputs of TGRs and WPGs at time t, respectively; $P_{g}^{\min}$ is the minimum power output of TGRs; RR_{g} is the maximum ramp rate of TGRs; TO_{g} and TS_{g} are the minimum online and offline time of TGRs, respectively; su_{g} and sd_{g} are the costs of single-time start-up and shut-down of TGR, respectively; ϕ_{n} is the set of bus nodes; $PTDF_{n,l}$ is the power transfer distribution factor; $F_{l}^{\max}$ is the power flow limit of the transmission line; $PFR_{g,t}^{\mathrm{G,nadir}}$ is the power increment headroom of TGRs for PFR at time t; σ_{g} is the PFR reserve factor, which is usually set to be 0.5; and $SFR_{g,t}^{\mathrm{G}}$, $rr_{g,t}$, $PFR_{g,t}^{\mathrm{G,QSS}}$, $d_{w,t}^{\mathrm{W}}$, $P_{w,t}^{\mathrm{W,MPPT}}$, $SFR_{w,t}^{\mathrm{W}}$, $PFR_{w,t}^{\mathrm{W,QSS}}$, $\Delta P_{\mathrm{loss},t}$, D_{t}^{sys}, R_{t}^{G}, $P_{n,t}^{\mathrm{L}}$, $P_{g,n,t}^{\mathrm{G}}$, and $P_{w,n,t}^{\mathrm{W}}$ are the values of the corresponding variables at time t.

Constraint (28) limits the minimum and maximum power outputs of TGRs and (29) limits the ramp rate in adjacent periods. Constraints (30) and (31) limit the minimum start-up and shut-down time for TGRs, while (32)-(34) calculate the corresponding costs. Constraint (35) ensures the system power balance and (36) limits the power flow of each transmission line. Constraints (37)-(40) ensure that the TGRs have sufficient power headroom to provide PFR and SFR. Constraint (41) calculates the actual output of WPGs after deloading, while (42) limits the output power of WPGs after participating in the PFR and SFR. Formulas (43)-(46) are the frequency security constraints, which are RoCoF constraint, frequency nadir constraint, QSS frequency deviation constraint, and SFR constraint, respectively. Note that although the uncertainties from RESs and load are considered in scheduling models or market pricing using different methods such as stochastic [34], robust [35], and chance-constrained [36] methods in other studies, these methods are not applied or discussed in this paper as uncertainty is not the focus of this work.

B. Linearization of Frequency Nadir Constraints

It is noted that the frequency nadir constraint is highly nonlinear, which is usually detrimental for solving as well as market pricing. In previous research, this is usually handled by a mixed-integer quadratic programming based PWL algorithm [37]. However, when the number of sampling points or fitting hyperplanes is slightly increased, the computational efficiency of this algorithm will be significantly degraded, which makes it difficult to apply to the practical scheduling process. For this reason, a mixed-integer linear programming (MILP) based PWL algorithm proposed in [29] is adopted for acceleration, which is given as:

$$\begin{cases} \min \sum_{e \in N_e} (t_{N_j} - g(H_{s,e}^{sys}, R_e^{sys}, F_{H,e}, D_e^{sys})) \\ \text{s.t. } t_{N_j} - g(H_{s,e}^{sys}, R_e^{sys}, F_{H,e}, D_e^{sys}) \ge 0 \quad e = 1,2,\ldots,N_e \\ \qquad \bar{g}_j(H_{s,e}^{sys}, R_e^{sys}, F_{H,e}, D_e^{sys}) \le t_j \quad j = 1,2,\ldots,N_j, e = 1,2,\ldots,N_e \\ \qquad t_j \le \bar{g}_j(H_{s,e}^{sys}, R_e^{sys}, F_{H,e}, D_e^{sys}) + v_j M \quad j = 1,2,\ldots,N_j, \\ \qquad\quad e = 1,2,\ldots,N_e \\ \qquad t_{j-1} \le t_j \le t_{j-1} + (1 - v_j)M \quad j = 1,2,\ldots,N_j, e = 1,2,\ldots,N_e \end{cases} \tag{47}$$

where N_e and N_j are the numbers of sampling points and fitting hyperplanes, respectively; $g(H_{s,e}^{sys}, R_e^{sys}, F_{H,e}, D_e^{sys})$ is the original frequency nadir function; $H_{s,e}^{sys}$, R_e^{sys}, $F_{H,e}$, and D_e^{sys} are the values of the corresponding variables of sampling point e; t_j and v_j are the auxiliary decision variables produced by applying the Big-M method; M is a large number; and $\bar{g}_j(H_{s,e}^{sys}, R_e^{sys}, F_{H,e}, D_e^{sys})$ is the additional decision variable representing the fitted linearized function with the following expression:

$$\bar{g}_j(H_{s,e}^{sys}, R_e^{sys}, F_{H,e}, D_e^{sys}) = a^j H_{s,e}^{sys} + b^j R_e^{sys} + c^j F_{H,e} + d^j D_e^{sys} + e^j \tag{48}$$

where a^j, b^j, c^j, d^j, and e^j are the fitting coefficients. Then, the number of sampling points is chosen as 30 and the number of fitting hyperplanes is chosen as 4, and the values of F_H and D^{sys} are fixed to be 3 to visualize the results, as shown in Fig. SC1 in Supplementary Material C. It can be observed that through the linear approximation of four hyperplanes, the linearized fitting plane is basically coincident with the original function. In addition, the values of sampling points before and after linearization are compared in Fig. SC2 in Supplementary Material C, and the fitting errors are evaluated using root mean square error (RMSE). It can be found that the real values and linearized values are very close, with an RMSE of 0.1%, which is acceptable for the scheduling model. After linearization, the frequency nadir constraints are reformulated as:

$$a^j H_{s,t}^{sys} + b^j R_t^{sys} + c^j F_{H,t} + d^j D_t^{sys} + e^j \le \Delta f_{\max} \quad \forall t, \forall j \tag{49}$$

where $H_{s,t}^{sys}$, R_t^{sys}, and $F_{H,t}$ are the values of the corresponding variables at time t.

Up to this, the proposed FCUC model is fully transformed into an MILP problem, which can be solved efficiently with commercial solvers, e.g., Cplex and Gurobi.

IV. Differentiated Pricing Scheme

After determining the scheduling plan of generators, the prices of energy and FRSs are calculated. However, the existence of binary decision variables $u_{g,t}^G$ in the proposed FCUC model leads to the non-satisfaction of the strong duality theorem, and it is impossible to directly obtain the corresponding dual variables for pricing. Therefore, we adopt the dispatchable method to deal with the non-convexity [38]. The binary decision variables are relaxed into continuous forms, which is given as:

$$0 \le u_{g,t}^G \le 1 \quad \forall t, \forall g \tag{50}$$

Subsequently, the linear programming based FCUC is solved to derive prices, and the Lagrangian function L for this problem contains the following terms:

$$\begin{aligned} L = \sum_{t \in T} \Bigg\{ & \sum_{g \in \phi_g} C_g(P_{g,t}^G) + \lambda_0 \left(\sum_{g \in \phi_g} P_{g,t}^G + \sum_{w \in \phi_w} P_{w,t}^W - \sum_{n \in \phi_n} P_{n,t}^L \right) + \sum_l \lambda_{L,l} \left[\sum_{n \in \phi_n} PTDF_{n,l} \cdot (P_{g,n,t}^G + P_{w,n,t}^W - P_{n,t}^L) - F_l^{\max} \right] + \\ & \lambda_{RoCoF} \left[\frac{\Delta P_{loss,t}}{RoCoF_{\max}} - 2(H_{s,t}^G + H_{s,t}^{W,GFM}) \right] + \sum_j \lambda_{nadir,j} [a^j (H_{s,t}^G + H_{s,t}^{W,GFM} + H_{s,t}^{W,GFL}) + b^j R_t^{sys} + c^j F_{H,t} + d^j (D_t + R_t^W) + e^j - \Delta f_{\max}] + \\ & \lambda_{QSS} [\Delta P_{loss,t} - (D_t + R_t^W + R_t^G) \Delta f_{QSS}^{\max}] + \lambda_{SFR} \left[\Delta P_{loss,t} - \Delta f_{QSS}^{\max} (R_t^G + R_t^W) - \sum_{g \in \phi_g} SFR_{g,t}^G - \sum_{w \in \phi_w} SFR_{w,t}^W \right] \Bigg\} \end{aligned} \tag{51}$$

where λ_0, $\lambda_{L,l}$, λ_{RoCoF}, λ_{QSS}, λ_{SFR}, and $\lambda_{nadir,j}$, are the dual variables for constraints (35), (36), (43), (45), (46), and (49), respectively; D_t is the aggregated load damping factor at time t; and $H_{s,t}^{W,GFM}$, $H_{s,t}^G$, $H_{s,t}^{W,GFL}$, and R_t^W are the values of the corresponding variables at time t. The price for each type of service is equal to the partial derivative of the Lagrangian function with respect to the increased demand for that service. Thus, the LMP at node n and time t $LMP_{n,t}$ can be derived as:

$$LMP_{n,t} = \lambda_0 + \sum_l \lambda_{L,l} \cdot PTDF_{n,l} \tag{52}$$

The LMP contains the energy component λ_0 and the congestion component $\sum_l \lambda_{L,l} \cdot PTDF_{n,l}$. The synchronous inertia provided by TGRs shares the same price as the inertia provided by GFM inverters since they contribute equally to the frequency dynamics, containing the RoCoF component $2\lambda_{\text{RoCoF}}$ and the nadir component $\sum_j \lambda_{\text{nadir},j} a^j$.

$$Pr_t^{H^{\text{G}}} = Pr_t^{H_{\text{s}}^{\text{W,GFM}}} = 2\lambda_{\text{RoCoF}} + \sum_j \lambda_{\text{nadir},j} a^j \tag{53}$$

where $Pr_t^{H^{\text{G}}}$ and $Pr_t^{H_{\text{s}}^{\text{W,GFM}}}$ are the inertia prices of TGRs and GFM inverters, respectively. The inertia provided by the GFL inverters only contributes to the frequency nadir, so its price $Pr_t^{H_{\text{s}}^{\text{W,GFL}}}$ includes only the nadir component.

$$Pr_t^{H_{\text{s}}^{\text{W,GFL}}} = \sum_j \lambda_{\text{nadir},j} a^j \tag{54}$$

where $Pr_t^{H_{\text{s}}^{\text{W,GFL}}}$ is the inertia price of GFL inverters.

The price of the PFR service provided by TGRs $Pr_t^{R^{\text{G}}}$ contains the nadir component $\sum_j \lambda_{\text{nadir},j} b^j$, the QSS component $\Delta f_{\text{QSS}}^{\max} \lambda_{\text{QSS}}$, and the SFR component $\Delta f_{\text{QSS}}^{\max} \lambda_{\text{SFR}}$ since the QSS frequency deviation directly affects the requirement of the SFR service:

$$Pr_t^{R^{\text{G}}} = \sum_j \lambda_{\text{nadir},j} b^j + \Delta f_{\text{QSS}}^{\max} \lambda_{\text{QSS}} + \Delta f_{\text{QSS}}^{\max} \lambda_{\text{SFR}} \tag{55}$$

Similarly, the price of the EFR service provided by WPGs $Pr_t^{R^{\text{W}}}$ also contains the above three components. Different from the PFR service, the regulation speed of EFR service provided by WPGs is faster, which has been endogenously distinguished by the PWL coefficients b^j and d^j:

$$Pr_t^{R^{\text{W}}} = \sum_j \lambda_{\text{nadir},j} d^j + \Delta f_{\text{QSS}}^{\max} \lambda_{\text{QSS}} + \Delta f_{\text{QSS}}^{\max} \lambda_{\text{SFR}} \tag{56}$$

The price for SFR service Pr_t^{SFR} can be calculated as:

$$Pr_t^{\text{SFR}} = \lambda_{\text{SFR}} \tag{57}$$

Subsequently, the revenue of TGRs Rev_g is derived as (58), including revenues from energy, inertia, PFR, and SFR:

$$Rev_g = (LMP_{n,t} \cdot P_{g,t}^{\text{G}} + Pr_t^{H^{\text{G}}} \cdot H_{\text{s},t}^{\text{G}} + Pr_t^{R^{\text{G}}} \cdot R_{g,t}^{\text{G}} + Pr_t^{\text{SFR}} \cdot SFR_{g,t}^{\text{G}}) \tag{58}$$

The revenue of GFM inverters Rev_w^{GFM} is derived as:

$$Rev_w^{\text{GFM}} = (LMP_{n,t} \cdot P_{w,t}^{\text{W}} + Pr_t^{H_{\text{s}}^{\text{W,GFM}}} \cdot H_{\text{s},t}^{\text{W}} + Pr_t^{R^{\text{W}}} \cdot R_{w,t}^{\text{W}} + Pr_t^{\text{SFR}} \cdot SFR_{w,t}^{\text{W}}) \tag{59}$$

The revenue of GFL inverters Rev_w^{GFL} is derived as:

$$Rev_w^{\text{GFL}} = (LMP_{n,t} \cdot P_{w,t}^{\text{W}} + Pr_t^{H_{\text{s}}^{\text{W,GFL}}} \cdot H_{\text{s},t}^{\text{W}} + Pr_t^{R^{\text{W}}} \cdot R_{w,t}^{\text{W}} + Pr_t^{\text{SFR}} \cdot SFR_{w,t}^{\text{W}}) \tag{60}$$

Finally, the profit can be calculated for each type of generator. The profits of TGRs are equal to their revenues minus the costs of generation, and the profits of GFM inverters and GFL inverters are equal to the revenues because of their zero marginal cost of generation, which are given as:

$$Profit_g = Rev_g - (C_g(P_{g,t}^{\text{G}}) + SU_{g,t} + SD_{g,t}) \tag{61}$$

$$Profit_w^{\text{GFM}} = Rev_w^{\text{GFM}} \tag{62}$$

$$Profit_w^{\text{GFL}} = Rev_w^{\text{GFL}} \tag{63}$$

where $Profit_g$, $Profit_w^{\text{GFM}}$, and $Profit_w^{\text{GFL}}$ are the profits of TGRs, GFM inverters, and GFL inverters, respectively.

V. Case Study

In this section, a modified IEEE 6-bus system and a modified IEEE RTS-79 system are applied to verify the effectiveness of the proposed method. The basic parameters of the two test systems are set as: the frequency security limits $RoCoF_{\max}$, $\Delta f_{\max}$, $\Delta f_{\text{QSS}}^{\max}$ are set to be 0.5 Hz/s, 0.8 Hz, and 0.5 Hz, respectively [27]. The maximum allowable deloading rate of WPG is set to be 30%, and the rotor speed reduction factor is set to be 0.2. The permanent magnet synchronous generator (PMSG) based WPG is used for the frequency support capability assessment, and the detailed parameters can be found in Table SCI in Supplementary Material C [29]. All of the models are implemented in MATLAB 2018 and solved by Gurobi 11.0.1 on a PC equipped with an Intel Core i7 processor and 16 GB of RAM. In addition, the following four scheduling cases are set up for comparison.

1) Case A: security-constrained UC model without frequency constraints.

2) Case B: FCUC model without the frequency support from WPGs.

3) Case C: FCUC model with the frequency support from WPGs, while the frequency response characteristics are modeled as fixed inertia and droop factors.

4) Case D: the proposed FCUC model with flexible frequency support from WPGs.

A. Modified IEEE 6-bus System

The topology of the modified IEEE 6-bus system is depicted in Fig. SC3 in Supplementary Material C, which contains four TGRs and two WFs. The total installed capacity of TGRs is 750 MW. The WPGs in WF1 are equipped with GFM inverters while those in WF2 are equipped with GFL inverters and the installed capacities of WF1 and WF2 are set to be 300 MW and 250 MW, respectively, with an installation penetration rate of 42.3%. Figure SC4 in Supplementary Material C shows the load curve and WF output curves. The daily peak load reaches 576 MW, and the maximum net load is 268 MW. During each period, the hypothetical power disturbance is set to be 10% of the total load demand. Specific parameters of TGRs and transmission lines can be found in [39].

1) Scheduling and Pricing Results

The total cost, revenue, and profit of each case is shown in Table I. Case A has the lowest scheduling cost since the frequency security constraints are not included. The TGRs are online only for the purpose of providing energy. It can also be observed from the UC results given in Fig. 3 that two TGRs are online during the period of 5th-22th hours, and only one TGR is online during the rest of the periods. However, the clearing results may not be able to resist the potential frequency disturbance. Case B adds the frequency security constraints, while the FRSs are only provided by the TGRs. It can be observed that the total cost of case B is increased by \$80038 while the profit of the WPGs decreases by \$90593. The negative profit of TGRs is observed because some of the TGRs are additionally started up and are operating at the minimum technical output to maintain the frequency security, which reduces the rate of wind power consumption and simultaneously leads to the energy price being much lower than the fuel cost of TGRs. Even though TGRs can benefit from the FR market, this revenue does not offset their generation cost.

TABLE I
COMPARISON OF TOTAL COST, REVENUE, AND PROFIT OF FOUR CASES IN MODIFIED IEEE 6-BUS SYSTEM

Case	Total cost ($)	Revenue and profit of TGR ($)					Revenue and profit of WPG ($)					
		Energy revenue	Inertia revenue	PFR revenue	SFR revenue	Profit	Energy revenue	Inertia revenue of GFM	Inertia revenue of GFL	EFR revenue	SFR revenue	Profit
Case A	56573	59693				3120	140418					140418
Case B	136611	33122	37324	57994	0	–8171	49825					49825
Case C	136858	69434	53963	23018	244	9801	100346	9855	2316	14780	223	127520
Case D	59836	59291	7619	8259	187	15520	128321	5953	987	7605	391	143257

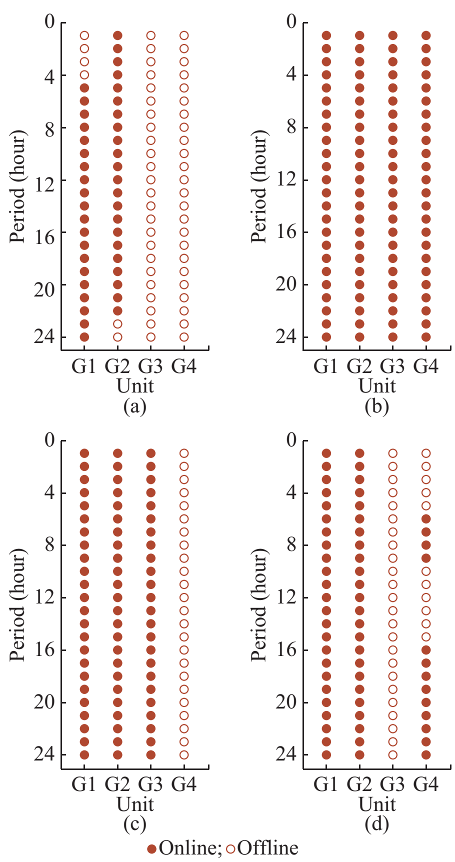

Fig. 3. Comparison of UC results. (a) Case A. (b) Case B. (c) Case C. (d) Case D.

Case C considers the FRSs from WPGs with fixed FR factors, which implies that WPGs are required to maintain a fixed amount of deloading rate during the full scheduling period. The profits of TGRs and WPGs in case C are increased compared with those in case B, and the number of online TGRs is reduced, with unit G4 shut down throughout the whole period. However, it is worth noting that the total cost of case C is rather higher than that of case B by $247. This is because the participation of WPGs in the form of fixed FR factors forces them to curtail output unreasonably during certain periods, such as some periods when the demand for FR is not strong but the energy supply requirements are high (period of the 9th hour). This directly leads to an additional increase in the output of TGRs, and in turn increases the scheduling cost. Compared with that of case C, the total cost of case D is reduced by $77022, and the profits of TGRs and WPGs are increased by $5719 and $15737, respectively. The largest unit G3 is shut down during all periods. This is because the designed market mechanism allows WPGs to provide dynamically matched inertia and FR capacity in an optimal way, which can improve the profitability of all participants while reducing the scheduling cost of the system. This also provides an incentive for all types of generators to participate actively in the FR market.

Figure 4 compares the daily generation mix of each case, and it can be observed that case A has the highest utilization of wind power as it does not require additional start-up of TGRs for frequency security.

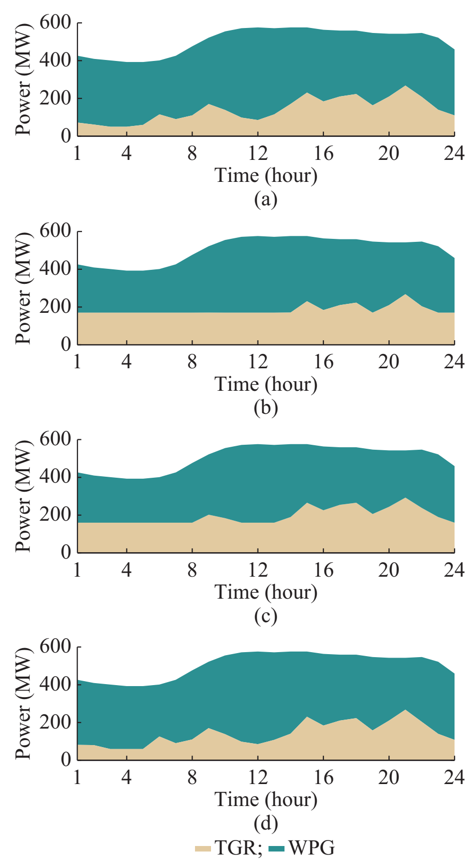

Fig. 4. Comparison of daily generation mix. (a) Case A. (b) Case B. (c) Case C. (d) Case D.

The utilization of wind power is significantly decreased in case B and case C, especially during the period of 1st-14th hours. Even though the WPG has a high available capacity during these periods, the TGRs are started up to meet the security requirements. The utilization of wind power in case D is similar to that in case A. It can also be observed from the deloading rate comparisons given in Fig. 5 that the deloading rates of the WFs in case C are all kept at 10% during the scheduling period since the dynamical deloading is not allowed. In case D, the deloading rate of WF1 is varied and that of WF2 is kept at the deloading rate limit. This is because the proposed method allows flexible deloading of WPGs for FR, which allows WPGs to make optimal decisions under different load demands and frequency security requirements, and reduces the start-up time of TGRs, thus improving the wind power accommodation.

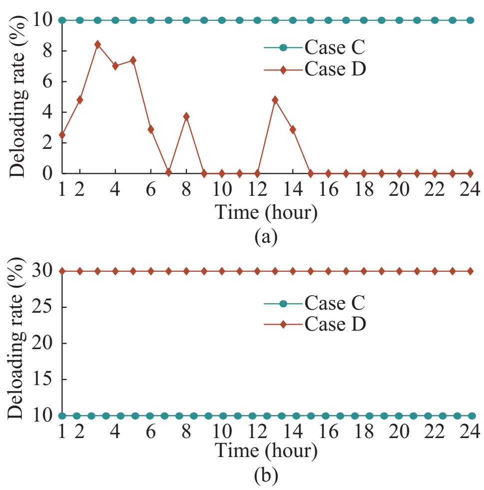

Fig. 5. Comparison of deloading rate of WFs in case C and case D. (a) Deloading rate of WF1. (b) Deloading rate of WF2.

Figures 6 and 7 compare the prices of various services in each case, all of which are obtained using the proposed differentiated pricing scheme. In case A, only the energy price is generated because it does not contain frequency security constraints. In case B, only the TGR inertia price, PFR price, and SFR price are obtained since only TGRs provide FRSs. In case C and case D, the GFM inverters are assigned the same inertia price with the TGRs because of their similar contribution to frequency dynamics, whereas the GFL inverter generates a separate inertia price. Furthermore, the prices of PFR and EFR differ according to the response speed differences. The EFR can be used to provide faster FR, and thus its price is higher than that of the PFR in both cases. For the SFR price, case B has a price of zero during all scheduling periods because all TGRs are online and the reserves for SFR are sufficient. The above analysis indicates that the proposed differentiated pricing scheme can reasonably price different FRSs according to the characteristics of various types of resources.

2) Comparison of Frequency Dynamics

To further illustrate the effectiveness of the proposed method, an equivalent simulation model is built based on MATLAB/Simulink to verify the frequency security in each case.

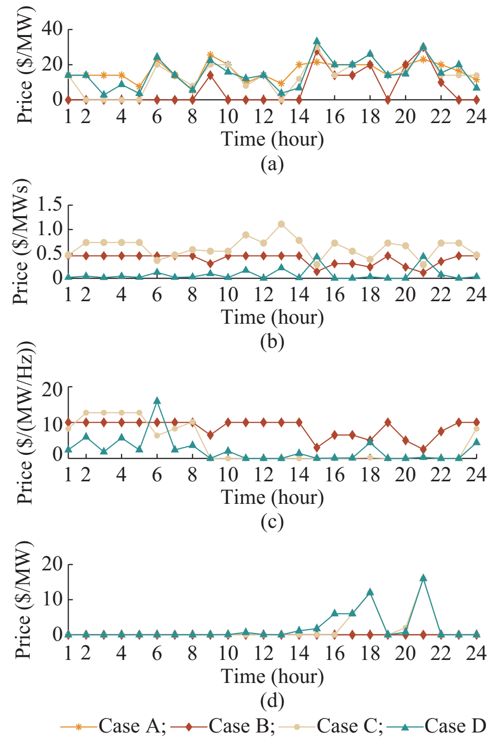

Fig. 6. Comparison of daily energy price, inertia price for TGR and GFM inverter, PFR price, and SFR price. (a) Energy price. (b) Inertia price for TGR and GFM inverter. (c) PFR price. (d) SFR price.

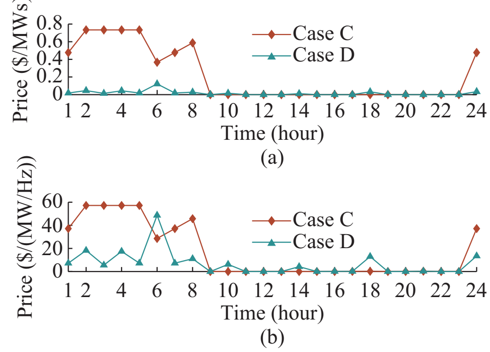

Fig. 7. Comparison of daily inertia price for GFL inverter and EFR price. (a) Inertia price for GFL inverter. (b) EFR price.

The comparison of RoCoF and frequency nadir of each case is shown in Fig. 8. In case A, it can be observed that the RoCoF exceeds the limit during all periods, and the frequency nadir exceeds the limit during the periods of 1st-4th, 11th-16th, and 23rd-24th hours, while in the other cases, the metrics are within the limits, which reflects the effectiveness of the frequency security constraints. Figure 9 shows a more detailed comparison of frequency dynamics of each case at the 24th hour. It can be found that at the beginning of the frequency disturbance, the frequency in case A falls rapidly, with the frequency nadir reaching 48.72 Hz and the QSS frequency deviation reaching 49.44 Hz, both of which do not meet the security requirements. In addition, it is worth noting that the frequency nadir of case D is slightly lower compared with that of case B and case C, which is because more TGRs are started up in case B and case C, and the inertia and PFR factors of TGRs are fixed values. Although the system frequency security is guaranteed, the additional start-up of TGRs may cause over-scheduling of FR resources and the loss of marginal price signals. The above results show that under the market scheduling model designed in this paper, both TGRs and WPGs can obtain excellent profits while guaranteeing frequency security.

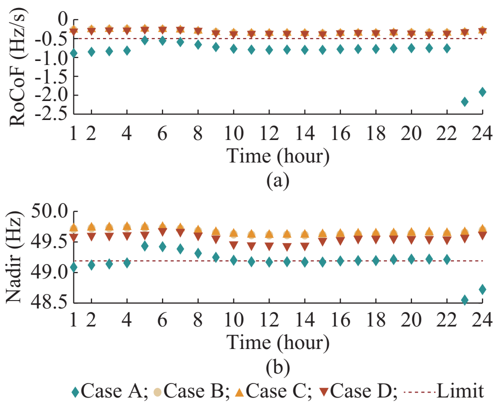

Fig. 8. Comparison of RoCoF and frequency nadir. (a) RoCoF. (b) Frequency nadir.

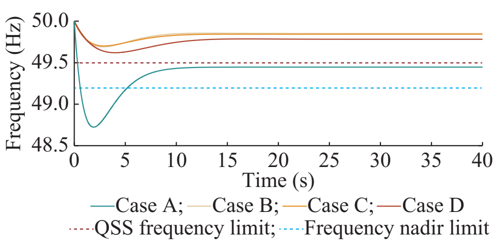

Fig. 9. Comparison of system frequency dynamics at 24th hour.

Additionally, we further evaluate the frequency security of each case using the frequency security margin proposed in [31]. The frequency security margin is defined as the maximum imbalance power that the scheduling result can tolerate. The results are shown in Fig. 10. It can be observed that the frequency security margin of case A is much lower than the system requirement, indicating that the system is highly susceptible to frequency instability under such scale of frequency disturbance. In contrast, the frequency security margins of the other cases, which consider frequency security constraints, are all above the system requirements, especially during the period of 1st-8th hours, which means that these cases have sufficient margins to withstand additional frequency disturbances. The above results also reflect the effectiveness of the proposed market scheduling model in enhancing the system frequency response capability from another perspective.

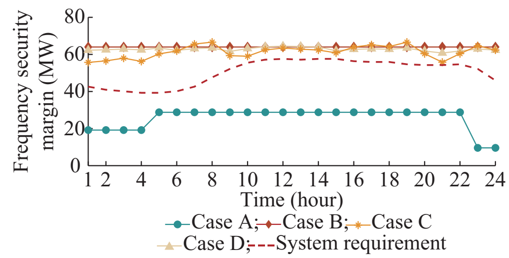

Fig. 10. Comparison of frequency security margin.

B. Modified IEEE RTS-79 System

The effectiveness and scalability of the proposed method are further tested in a modified IEEE RTS-79 system. The installed capacity of TGRs is 2391 MW. The total installed capacity of WPGs is 2500 MW, with the installation number of GFM inverters and GFL inverters each accounting for 50%, and the installation penetration rate of WPGs reaches 51.1%. The daily peak load is 2845.5 MW. 200 MW of hypothetical power disturbance is set for each period. The topology of the test system and the parameters of TGRs and transmission lines can be found in [40].

1) Scheduling Results

The scheduling results are summarized in Table II and Fig. 11.

TABLE II
COMPARISON OF TOTAL COST, REVENUE, AND PROFIT OF FOUR CASES IN MODIFIED IEEE RTS-79 SYSTEM

Case	Total cost ($\$10^5$)	Revenue and profit of TGR ($\$10^5$)					Revenue and profit of WPG ($\$10^5$)					
		Energy revenue	Inertia revenue	PFR revenue	SFR revenue	Profit	Energy revenue	Inertia revenue of GFM	Inertia revenue of GFL	EFR revenue	SFR revenue	Profit
Case A	1.91	3.29				1.38	5.86					5.86
Case B	6.61	1.28	10.34	0.0016	0.0161	5.04	2.12					2.12
Case C	5.19	4.65	5.92	0.0030	0.0105	5.39	6.64	1.347	0	0.0001	0.025	8.01
Case D	2.76	5.32	0.41	0.0081	0.0156	2.99	8.83	0.540	0	0.0031	0.122	9.49

It can be observed that case D has the lowest total cost and the highest profit for WPGs among all cases that consider the frequency security constraints. In Fig. 11, it can be observed that case A has the lowest number of online TGRs, while case B has the highest, which is maintained at 12 online TGRs throughout the day. The number of online TGRs of case D is close to that of case A, with only 8 online TGRs at most, which also demonstrates that the proposed method can effectively optimize the number of online TGRs and promote the utilization of wind power. Moreover, we notice that the PFR, EFR, and SFR revenues of each case are much smaller than the inertia revenues. This is because the RoCoF constraint is the dominant constraint, and the system inertia requirement is much higher than the PFR, EFR, and SFR requirements. This suggests that inertia services are scarcer and more generators are online for the purpose of providing inertia, which also illustrates the effectiveness of the proposed differentiated pricing scheme.

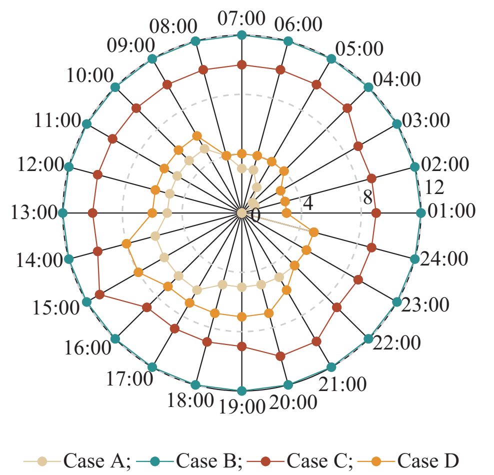

Fig. 11. Comparison of number of online TGRs.

2) Impact of Installation of GFM and GFL Inverters

The impact of the installation of GFM and GFL inverters is studied. The total installed capacity of WPGs remains 2500 MW, and only the installation rate of GFM inverters is changed to simulate the transformation process from GFL inverters to GFM inverters. From Fig. 12, it can be found that as the installation rate of GFM inverters increases, the total cost decreases by 39.1%, and the profit and the load serving rate of WF are improved by 50.9% and 3.9%, respectively.

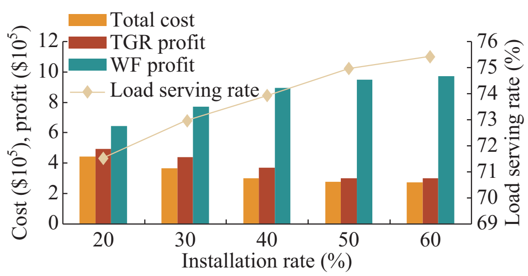

Fig. 12. Impact of installation rate of GFM inverters.

This is because as more GFM inverters are equipped, the inertia provided by WPGs becomes more valuable, which reduces the start-up times of TGRs, and thereby improves the utilization of wind power, suggesting a greater competitive advantage in the electricity market compared with GFL inverters. The above results also show that the proposed method can guarantee that the GFM inverters receive sufficient economic incentives to facilitate the transition from GFL inverters to GFM inverters, while also ensuring the frequency security under the existing installed capacity of GFL inverters.

3) Sensitivity to Installation of Wind Power

Figure 13 compares the total cost and load serving rate between case C and case D with different wind power installations. It can be observed that with the increase of wind power installation, the total cost of both cases decreases and the load serving rate increases, because more wind power with zero marginal generation cost is prioritized for scheduling. However, it is important to note that a higher wind power installation also introduces greater uncertainty into the system. This increase in uncertainty can impact system stability and may require additional balancing resources to maintain secure operations, which may partially reduce the cost savings observed here. In addition, it can be found that the total cost of case D is lower than that of case C, and the load serving rate is higher when the same wind power installation is considered, which is because the proposed method allows the dynamic frequency support of WPGs to select the optimal deloading rate.

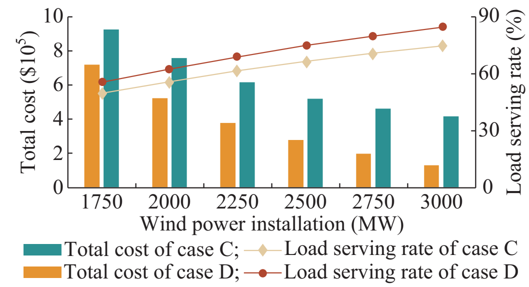

Fig. 13. Impact of wind power installation on total cost and load serving rate.

4) Sensitivity to System Frequency Security Limits

The impact of the system frequency security limits on the system scheduling and pricing results is studied. The RoCoF and frequency nadir metrics are selected as they are usually the dominant constraints. The results are depicted in Fig. 14 and Fig. 15. It can be observed that when the RoCoF constraint is tight, the system inertia price is very high, and the PFR price is zero during most of the periods. This is because the RoCoF constraint is much more binding than the rest of the frequency security constraints, and the system inertia is scarcer. With the gradual relaxation of RoCoF, the system scheduling cost is significantly reduced, and the load serving rate of WF increases from 71.7% to 75.7%. The inertia price is gradually reduced to zero, especially when RoCoF is relaxed to 0.5 Hz/s, and the inertia price is equal to zero during almost all the periods, which indicates that the RoCoF constraints have lost the binding force.

In terms of the frequency nadir limit, similar conclusions can be obtained as the RoCoF limit. In addition, it can be intuitively observed from Fig. 15 that the inertia price of GFL inverters is always lower than that of TGRs and GFM inverters under the same frequency nadir limit because the inertia of GFL inverters does not contribute to the RoCoF. The PFR price is also always lower than the EFR price because EFR has a faster regulation speed and contributes more to the frequency dynamics. This shows that the proposed differentiated pricing scheme can reflect the actual value of each type of resource, and motivate generators with higher response quality to participate in FR, thus better improving the system frequency security.

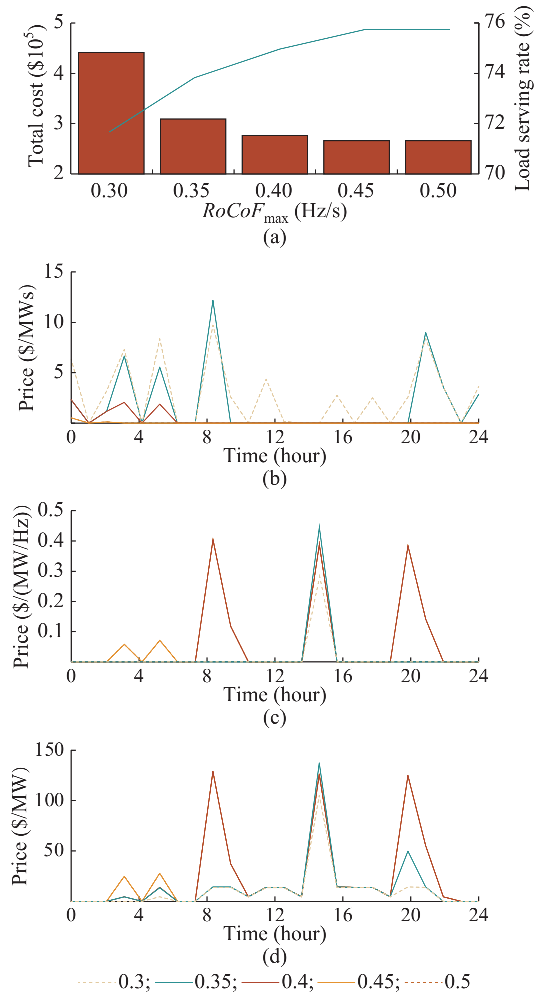

Fig. 14. Total cost, load serving rate of WF, and market prices under different RoCoF limits. (a) Total cost and load serving rate of WF. (b) Inertia price for TGR and GFM inverter. (c) PFR price. (d) Energy price.

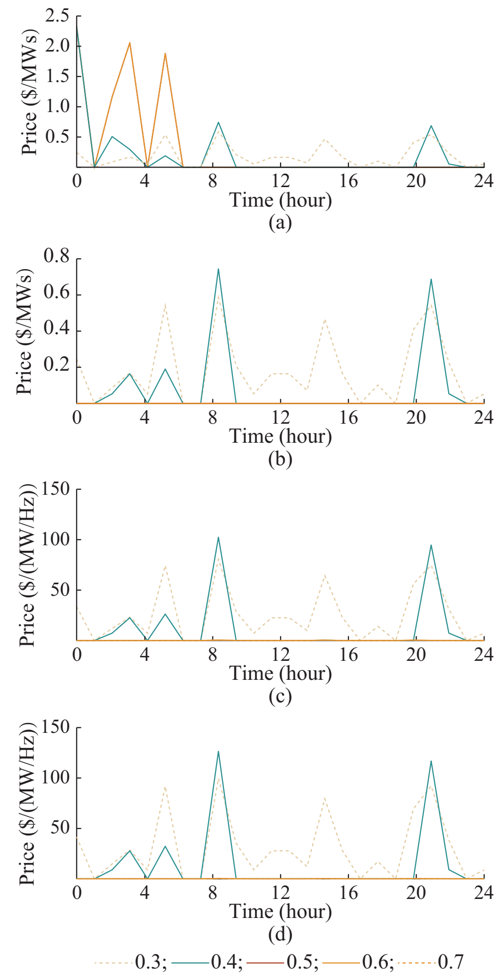

Fig. 15. Market prices under different frequency nadir limits. (a) Inertia price for TGR and GFM inverter. (b) Inertia price for GFL inverter. (c) PFR price. (d) EFR price.

VI. Conclusion

In this paper, a market scheduling and pricing method for comprehensive FRSs is proposed to ensure frequency security in the renewable-dominant power system. Through the numerical simulations conducted on a modified IEEE 6-bus system and a modified IEEE RTS-79 system, the effectiveness of the proposed method is verified. The results suggest that:

1) The proposed modeling approach effectively reflects the flexible FR characteristics of WPGs under full wind speed conditions, allowing them to provide flexible and variable regulation services, so as to make a better trade-off between the energy market and the FR market. Compared with the existing research, the profit and utilization rate of wind power with the proposed method are increased by 18.5% and 8.5%, respectively.

2) The proposed frequency security constraint set of the whole FR process effectively distinguishes the contributions of different types of regulation resources and ensures the frequency security of the power system. The proposed differentiated pricing scheme can effectively combine the regulation quality for pricing and incentivize generators, especially WPGs, to participate in the FR market.

3) The results of the sensitivity analysis suggest that the FR performance of GFM inverters is better. Compared with that of GFL inverters, the profit space of GFM inverters in the FR market is larger. Moreover, the system frequency security limits can affect the clearing results as well as the prices, and the system operator should take into account the actual operating conditions and set the limits reasonably.

Future work will focus on the modeling of the uncertainty pertaining to RESs and load in market scheduling and pricing. Related uncertainty modeling methods such as stochastic programming and robust optimization can lead to nonconvex models, resulting in difficulties in solving and pricing. Addressing these uncertainties and the resulting non-convexities can effectively enhance the reliability of scheduling and pricing results in practical applications, facilitating better integration of RESs.

References

[1] J. Li, Y. Qiao, Z. Lu *et al.*, "Integrated frequency-constrained scheduling considering coordination of frequency regulation capabilities from multi-source converters," *Journal of Modern Power Systems and Clean Energy*, vol. 12, no. 1, pp. 261-274, Jan. 2024.

[2] B. Wang, D. Yang, G. Cai *et al.*, "Online inertia estimation using electromechanical oscillation modal extracted from synchronized ambient

data," *Journal of Modern Power Systems and Clean Energy*, vol. 10, no. 1, pp. 241-244, Jan. 2022.

[3] K. Yan, G. Li, R. Zhang *et al*., "Frequency control and optimal operation of low-inertia power systems with HVDC and renewable energy: a review," *IEEE Transactions on Power Systems*, vol. 39, no. 2, pp. 4279-4295, Mar. 2024.

[4] J. Hu, Z. Yan, X. Xu *et al*., "Inertia market: mechanism design and its impact on generation mix," *Journal of Modern Power Systems and Clean Energy*, vol. 11, no. 3, pp. 744-756, May 2023.

[5] Z. Wu, W. Gao, T. Gao *et al*., "State-of-the-art review on frequency response of wind power plants in power systems," *Journal of Modern Power Systems and Clean Energy*, vol. 6, no. 1, pp. 1-16, Jan. 2018.

[6] Y. Wang, X. Gu, Y. Bai *et al*., "DDPG based coordinated control strategy of wind-PV-storage system for long-term restoration process," *IEEE Transactions on Industry Applications*, vol. 61, no. 2, pp. 2620-2631, Mar. 2025.

[7] F. D. Galiana, F. Bouffard, J. M. Arroyo *et al*., "Scheduling and pricing of coupled energy and primary, secondary, and tertiary reserves," *Proceedings of the IEEE*, vol. 93, no. 11, pp. 1970-1983, Nov. 2005.

[8] E. Ela, V. Gevorgian, A. Tuohy *et al*., "Market designs for the primary frequency response ancillary service – part I: motivation and design," *IEEE Transactions on Power Systems*, vol. 29, no. 1, pp. 421-431, Jan. 2014.

[9] E. Ela, V. Gevorgian, A. Tuohy *et al*., "Market designs for the primary frequency response ancillary service – part II: case studies," *IEEE Transactions on Power Systems*, vol. 29, no. 1, pp. 432-440, Jan. 2014.

[10] G. Zhang, E. Ela, and Q. Wang, "Market scheduling and pricing for primary and secondary frequency reserve," *IEEE Transactions on Power Systems*, vol. 34, no. 4, pp. 2914-2924, Jul. 2019.

[11] H. Chavez, R. Baldick, and S. Sharma, "Governor rate-constrained OPF for primary frequency control adequacy," *IEEE Transactions on Power Systems*, vol. 29, no. 3, pp. 1473-1480, May 2014.

[12] B. Chen, R. Khatami, A. Al-Digs *et al*., "Incorporating system frequency dynamics into real-time locational marginal pricing of electricity," *IEEE Transactions on Power Systems*, vol. 39, no. 2, pp. 4638-4649, Mar. 2024.

[13] E. Saiz-Marin, J. Garcia-Gonzalez, J. Barquin *et al*., "Economic assessment of the participation of wind generation in the secondary regulation market," *IEEE Transactions on Power Systems*, vol. 27, no. 2, pp. 866-874, May 2012.

[14] K. Li, H. Guo, X. Fang *et al*., "Market mechanism design of inertia and primary frequency response with consideration of energy market," *IEEE Transactions on Power Systems*, vol. 38, no. 6, pp. 5701-5713, Nov. 2023.

[15] Z. Liang, R. Mieth, and Y. Dvorkin, "Inertia pricing in stochastic electricity markets," *IEEE Transactions on Power Systems*, vol. 38, no. 3, pp. 2071-2084, May 2023.

[16] L. Badesa, F. Teng, and G. Strbac, "Pricing inertia and frequency response with diverse dynamics in a mixed-integer second-order cone programming formulation," *Applied Energy*, vol. 260, p. 114334, Feb. 2020.

[17] X. Zhang, T. Tan, B. Zhou *et al*., "Adaptive distributed auction-based algorithm for optimal mileage based AGC dispatch with high participation of renewable energy," *International Journal of Electrical Power & Energy Systems*, vol. 124, p. 106371, Jan. 2021.

[18] Z. Li, Z. Cheng, Y. Wang *et al*., "Distributed event-triggered fixed-time SMC-based AGC for power systems with heterogeneous frequency regulation units," *IEEE Transactions on Industrial Informatics*, vol. 20, no. 5, pp. 8031-8043, May 2024.

[19] J. Bjork, D. Pombo, and K. H. Johansson, "Variable-speed wind turbine control designed for coordinated fast frequency reserves," *IEEE Transactions on Power Systems*, vol. 37, no. 2, pp. 1471-1481, Mar. 2022.

[20] H. Gao, H. Xin, L. Huang *et al*., "Common-mode frequency in converter-integrated power systems: definition, analysis, and quantitative evaluation," *IEEE Transactions on Power Systems*, vol. 37, no. 6, pp. 4846-4860, Nov. 2022.

[21] W. Gu, Z. Chen, Q. Li *et al.*, "Torque limit-based inertial control method based on delayed support for primary frequency control of wind turbines," *Journal of Modern Power Systems and Clean Energy*, vol. 12, no. 2, pp. 561-570, Mar. 2024.

[22] R. Pan, D. Liu, S. Liu *et al.*, "Stability comparison between grid-forming and grid-following based wind farms integrated MMC-HVDC," *Journal of Modern Power Systems and Clean Energy*, vol. 11, no. 4, pp. 1341-1355, Jul. 2023.

[23] H. Zhang, W. Xiang, W. Lin *et al*., "Grid forming converters in renewable energy sources dominated power grid: control strategy, stability, application, and challenges," *Journal of Modern Power Systems and Clean Energy*, vol. 9, no. 6, pp. 1239-1256, Nov. 2021.

[24] B. K. Poolla, D. Gros, and F. Dorfler, "Placement and implementation of grid-forming and grid-following virtual inertia and fast frequency response," *IEEE Transactions on Power Systems*, vol. 34, no. 4, pp. 3035-3046, Jul. 2019.

[25] L. Badesa, C. Matamala, Y. Zhou *et al*., "Assigning shadow prices to synthetic inertia and frequency response reserves from renewable energy sources," *IEEE Transactions on Sustainable Energy*, vol. 14, no. 1, pp. 12-26, Jan. 2023.

[26] R. Prasad and N. P. Padhy, "Synergistic frequency regulation control mechanism for DFIG wind turbines with optimal pitch dynamics," *IEEE Transactions on Power Systems*, vol. 35, no. 4, pp. 3181-3191, Jul. 2020.

[27] Z. Chu, U. Markovic, G. Hug *et al*., "Towards optimal system scheduling with synthetic inertia provision from wind turbines," *IEEE Transactions on Power Systems*, vol. 35, no. 5, pp. 4056-4066, Sept. 2020.

[28] H. Li, Y. Qiao, Z. Lu *et al*., "Frequency-constrained stochastic planning towards a high renewable target considering frequency response support from wind power," *IEEE Transactions on Power Systems*, vol. 36, no. 5, pp. 4632-4644, Sept. 2021.

[29] Y. Jiang, S. Zhao, H. Wang *et al*., "Distributionally robust frequency constrained unit commitment with frequency support of wind power and synchronous condenser," *Transactions of China Electrotechnical Society*, doi: 10.19595/j.cnki.1000-6753.tces.232164

[30] Q. Shi, F. Li, and H. Cui, "Analytical method to aggregate multi-machine SFR model with applications in power system dynamic studies," *IEEE Transactions on Power Systems*, vol. 33, no. 6, pp. 6355-6367, Nov. 2018.

[31] Z. Zhang, E. Du, F. Teng *et al*., "Modeling frequency dynamics in unit commitment with a high share of renewable energy," *IEEE Transactions on Power Systems*, vol. 35, no. 6, pp. 4383-4395, Nov. 2020.

[32] P. Kundur, *Power System Stability and Control*. New York, USA: McGraw-Hill, 1994.

[33] J. W. Simpson-Porco, "On area control errors, area injection errors, and textbook automatic generation control," *IEEE Transactions on Power Systems*, vol. 36, no. 1, pp. 557-560, Jan. 2021.

[34] S. Wong and J. D. Fuller, "Pricing energy and reserves using stochastic optimization in an alternative electricity market," *IEEE Transactions on Power Systems*, vol. 22, no. 2, pp. 631-638, May 2007.

[35] H. Ye, Y. Ge, M. Shahidehpour *et al*., "Uncertainty marginal price, transmission reserve, and day-ahead market clearing with robust unit commitment," *IEEE Transactions on Power Systems*, vol. 32, no. 3, pp. 1782-1795, May 2017.

[36] Y. Dvorkin, "A chance-constrained stochastic electricity market," *IEEE Transactions on Power Systems*, vol. 35, no. 4, pp. 2993-3003, Jul. 2020.

[37] H. Ahmadi and H. Ghasemi, "Security-constrained unit commitment with linearized system frequency limit constraints," *IEEE Transactions on Power Systems*, vol. 29, no. 4, pp. 1536-1545, Jul. 2014.

[38] M. Toulabi, "Improvement in frequency stability of power grids with high penetration of renewable energy sources: market-clearing and pricing of required ancillary services," *IEEE Transactions on Engineering Management*, vol. 70, no. 10, pp. 3385-3394, Oct. 2023.

[39] Q. Wang, J. P. Watson, and Y. Guan, "Two-stage robust optimization for $N-k$ contingency-constrained unit commitment," *IEEE Transactions on Power Systems*, vol. 28, no. 3, pp. 2366-2375, Aug. 2013.

[40] P. Subcommittee, "IEEE reliability test system," *IEEE Transactions on Power Apparatus and Systems*, vol. PAS-98, no. 6, pp. 2047-2054, Nov. 1979.

Yihang Jiang received the B.S. degree in electrical engineering from North China Electric Power University, Baoding, China, in 2022, where he is currently working toward the Ph.D. degree. His research interests include renewable energy integration, low-inertia power system operation, and uncertainty modeling.

Shuqiang Zhao received the B.S., M.S., and Ph.D. degrees in electrical engineering from North China Electric Power University, Beijing, China, in 1985, 1989, and 1999, respectively. He is currently a Professor in the Department of Electrical and Electronic Engineering, North China Electric Power University. His research interests include power system reliability analysis and power system operation and planning.